The Conversion of Helix H2 to β-Sheet Is Accelerated in the Monomer and Dimer of the Prion Protein upon T183A Mutation

Yassmine Chebaro and Philippe Derreumaux*

Laboratoire de Biochimie Théorique, UPR 9080 CNRS, Institut de Biologie Physico Chimique et Université Paris Diderot-Paris 7, 13 rue Pierre et Marie Curie, 75005 Paris, France

Received: January 13, 2009; Revised Manuscript Received: March 30, 2009

The conversion of the prion protein (PrP) from its cellular form, PrP^C, to its pathogenic scrapie form, PrP^{Sc}, is a key event in neurodegenerative transmissible spongiform encephalopathies such as Creutzfeldt−Jakob disease (CJD). PrP^C is characterized by three helices (H1−H3) and a small antiparallel β-sheet. One working hypothesis for TSE causation is that oligomeric forms of PrP are the proximate neurotoxic agents. Because these states are transient in character, current experimental studies have failed to provide atomic structures. To gain insights into these intermediates, we have studied PrP125-228 and its CJD-causing T183A variant in their monomer and dimer forms by means of coarse-grained protein molecular dynamics simulations. Our 1.5 microsecond simulations show that the decrease in the thermodynamic stability of PrP monomer upon T183A, consistent with experimental studies, results from a destabilization of the H2H3 subdomain. Comparison of the monomer and dimer properties from wild-type and T183A PrP reveals that helix H1 is robust and the H2H3 subdomain displays a much higher propensity for intra- and inter-β-sheets in T183A than in the wild-type sequence under denaturing conditions. However, both species display negligible β-sheet structure. Implications of our simulations on prion propagation are discussed.

1. Introduction

The post-translational conversion of the prion protein (PrP) from its cellular form, PrP^C, to its pathogenic scrapie form, PrP^{Sc}, is a key event at the origin of the neurodegenerative transmissible spongiform encephalopathies.[1] The product of the PrP gene, widely considered as the infectious agent, aggregates into cytotoxic oligomers and eventually amyloid fibers causing cell death. In vivo, mammalian PrP^C of 23−231 amino acids is anchored to the membrane by a glycosyl phosphatidyl inositol (GPI) at position Ser230 and carries two glycosylation sites at Asn181 and Asn197 (numbering of the human species). Its physiological function is not fully determined, but we know that PrP^C contributes to transport of copper, neuronal morphology and adhesion, and regulation of lymphocytes, among others.[2,3]

The PrP^C and PrP^{Sc} isoforms display distinct biophysical and biochemical properties: PrP^C is α-helical, soluble, and sensitive to proteinase K, while PrP^{Sc} is rich in β-structure, insoluble and partially resistant to proteinase K.[4] The structure of the recombinant PrP90-231, recPrP, has been characterized by NMR and X-ray crystallography for many mammalian species[5,6] and displays two regions: a flexible, disordered N-terminal tail spanning amino acids 90−123 and a C-terminal globular domain with three α-helices: H1 (144−153), H2 (172−192), and H3 (200−225) and a short two-stranded β-sheet: S1 (129−130) and S2 (162−163). There is time-resolved FTIR spectroscopy evidence that the structure of the membrane-anchored native PrP^C23−231 is similar to recPrP below a threshold concentration, in agreement with previous report,[7] but at higher concentration, PrP^C forms dimers and oligomers with an increase of β-sheet signal.[8] In contrast to recPrP, PrP^{Sc} oligomers and fibrils are not amenable to high-resolution structures because they are transient and insoluble in character, respectively.

Despite decades of study, the transition from PrP^C and PrP^{Sc} remains poorly understood. Although folding to the PrP^C isoform is under kinetic control,[9] and constraining the loop 166−175 releases prion infectivity,[10,11] little is known on the structure of the monomeric, dimeric or higher-order intermediates.[12] Regardless of the kinetic model for prion propagation (template-assisted or variants of the nucleation model) and the size of the nucleus, many studies have indicated a critical role of PrP dimers in the conversion process.[13−18]

A total of 30 mutations have been reported in the PrP gene.[19] Here, we study the heterozygous T183A mutation.[20] This mutation, located in helix H2, prevents glycosylation of Asn181 and leads to intracellular PrP^{Sc} deposits causing Creutzfeldt−Jakob disease (CJD).[21] By using biogenesis and maturation of PrP T183A in the secretory pathway of neuronal cells, Kiachopoulos et al. suggested that the defect of maturation in the T183A variant is likely caused by the destabilization of the hydrophobic C-terminal domain.[22] This hypothesis is in agreement with the decrease of 19.3 $kJ.mol^{-1}$ in the thermodynamical stability of the murine recPrP121-231 T183A variant with respect to wild-type murine recPrP121-231 as measured by urea-induced equilibrium transitions.[23] However, this destabilization does not lead to any significant change in recPrP structural characteristics as far-UV and near-UV CD spectra of both T183A and wild-type PrP are very similar at 298 K.[23]

The recombinant PrP, as a model of PrP^C, has been the subject of many molecular dynamics (MD) simulations using all-atom explicit solvent[24−32] and simplified[33] force fields in its monomeric form, but a single MD in its dimeric form.[34] Many simulations have also been reported on PrP fragments.[15,35−37] In this study, by using the coarse-grained protein OPEP force field incorporating an implicit solvent model, we investigate the effect of the T183A mutation on the structural and dynamical

* To whom correspondence should be addressed. E-mail: philippe.derreumaux@ibpc.fr.

10.1021/jp900334s CCC: $40.75
Published on Web 04/16/2009

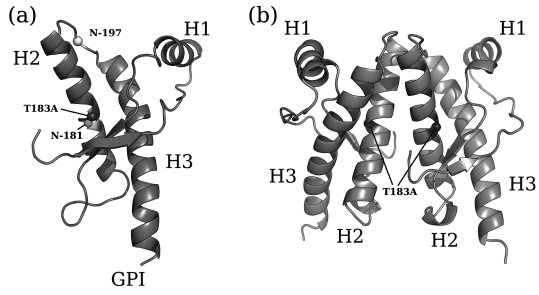

Figure 1. Starting structures of wild-type PrP125-228. (A) Monomer structure with the positions of the GPI anchor, the two glycosylation sites (N-181 and N-197), the T183A mutation, and the three native helices indicated. (B) Dimer structure with the positions of the T183A mutations.

properties of PrP125-228 monomer and dimer by means of MD simulations at various temperatures. We find that the conversion of the helix H2 to β-sheet is accelerated in the monomer and dimer of the prion protein upon T183A mutation, but both species display negligible β-sheet structure at low temperatures.

2. Materials and Methods

2.1. Coarse-Grained Force Field. In this work, the disulfide-bridge Cys179−Cys214 is treated at the united-atom level and parametrized with harmonic bond and bond-angle terms, and cosine dihedral terms taken from AMBER.[38] All other amino acids (except proline, where all heavy atoms are considered) use OPEP representation consisting of five particles for the main-chain (atoms N, C, O,, and C_α) and one bead for the side chain.[39,40] The side-chain bead is positioned at the center of mass of the heavy atoms and has appropriate van der Waals radius.[41] The coarse-grained OPEP force field, including short-range and long-range interactions, has been described in detail elsewhere.[41] Solvent effects are considered implicitly through the parameters of the hydrogen-bonding potential consisting of two-body and four-body terms, and the pairwise contact potential between side-chains represented by either a 12−6 potential or a repulsive −6 potential.

We use the OPEP version 3.2 parameter set optimized on a set of 29 proteins.[42] With this parameter set, basin-hopping simulations of the Aβ(21−30) monomer provide a very good structural fit with NMR,[43] MD simulations of two 46-residue and 56-residue proteins point to root-mean-square (rms) deviations of 2.0 Å from their NMR structures within 50 ns at 298 K,[41] and replica-exchange MD (REMD) simulations recover the experimental structures and thermodynamics of a 16-residue β-hairpin model and a 20-residue Trp-cage starting from randomly chosen states.[44] Simulations on oligomers of amyloid peptides were also found to share similar properties with all-atom simulations in explicit solvent.[45,46]

2.2. MD Simulations. The MD starting points for the wild-type monomer and dimer PrP, shown in Figure 1, are taken from the crystal structure of sheep PrP125-228 (PDB code 1UW3) with the C148 mutation restored to the wild-type R148.[47] The initial orientation of the chains in the dimer is thus that provided by X-ray crystallography.[47] The structures of the T183A variants are constructed using the Swiss-model program.[48] Although the amino acids 106−126 contribute to toxicity,[49,50] we use PrP125-228 because the N-terminal tail positions are not identified experimentally in recPrP and the effect of T183A on PrP stability is only known on the truncated mouse PrP121-231.

Prior to production, each model is minimized and equilibrated at the appropriate temperature for 1 ns. The trajectories at neutral pH are obtained with MD-OPEP[41] at constant temperature controlled by a Berendsen's bath. The algorithm RATTLE is used to constrain the vibration of bonds, allowing an integration time step of 1.5 fs.[44]

Here, the (wild-type, T183A) PrP monomer is subject to (one, two) 50 ns MD at 290 K, (one, two) 100 ns MD at 320 K and (two, three) 100 ns MD at 360 K, using different random seeds. The T183A PrP dimer is subject to three 60 ns MD at both 320 and 360 K, while the wild-type PrP dimer is studied by three 60 ns runs at 360 K. Note our temperatures are selected to explore PrP properties below and above the melting temperature of wild-type PrP, $T_m = 340$ K,[51] and our time scales of 100 ns for the monomer and 60 ns for the dimer are much longer than in most previous simulations, 10−20 ns[24,52] and 10 ns,[34] respectively.

2.3. Analysis. In this study, the first 30 ns of the monomer and 10 ns of the dimer trajectories are excluded from analysis. In what follows, we use PrP for recPrP for brievety. The MD are monitored using several order parameters: the C_α-rms deviations of residues 125−215 with respect to the minimized crystal structure and the C_α rms fluctuations of residues 125−228 with respect to the average MD structure. Following ref 53, the PrP structure is divided into the S1H1S2 and H2H3 subdomains spanning amino acids 125−171 and 172−215. Secondary structure composition is determined using the STRIDE program.[54] We also cluster the conformations by using the single linkage algorithm of the GROMACS 3.3.1 package[55] with a C_α-rmsd-based cutoff of 1.8 Å on residues 125−215 for both systems. Note that the C-terminal helix H3 encompassing amino acids 216−228 is excluded from the rms deviation as a function of time and the cluster analysis because of its known mobility as determined by NMR relaxation[56] and simulations.[26,53] The van der Waals contacts that disappear upon replacement of Thr183 by Ala183 are calculated using the criteria defined in ref 57.

3. Results

3.1. Impact of T183A on PrP Monomer at 290 and 320 K. The C_α-rms deviations of wild-type and T183A PrP at 290 K from their minimized crystal structures are shown in Figure 2a. At 50 ns, the rms deviation reaches 4 Å for wild-type PrP and 5.5 and 4.8 Å for T183A in runs 1 and 2. Secondary structure analysis in Table 1 and C_α-rms fluctuations with respect to the average MD structure in Figure 2b show that the three helices remain formed in the wild-type run and essentially formed in T183A run1 (H1 and H3 100%, H2 92.7%), but not in T183A run 2, where H3 averages 68%. The destabilization of the C-terminal amino acids 215−227 in run 2 does not impact, however, the subdomain H2H3 (rmsd of 2.0 Å) and the formation of S1 and S2 strands (see Table 1). By contrast, although helix H2 is essentially formed in T183A run 1, high mobility is observed in the S2−H2 loop (rms fluctuations reaching 3.3 Å at positions 167 and 173) and the C-terminal H2 helix (rmsd of 6 Å at position 193) and H2 helix is kinked at position 185.

Comparison of the PrP^C structure and dynamics from several mammalian species indicates, however, that all MD-OPEP deviations in T183A are seen in other species. For instance, the reduced helical character of the C-terminal helix H3 was determined on wild-type human Syrian hamster PrP using hydrogen exchange and NMR relaxation studies.[58] The high fluctuation in the C-terminal helix H2 of T183A was also observed in the NMR structure of human PrP125-228(S170N) where helix H2 spans 173−182.[59] The lower population of

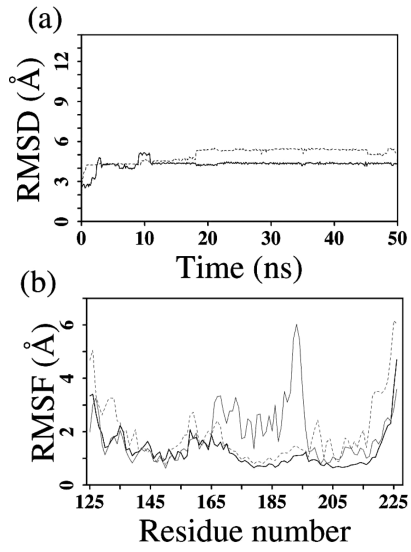

Figure 2. Wild-type and T183A monomer PrP properties at 290 K. (a) C_α-rmsd (in Å) from the minimized structure of the residues 129−215 for the wild-type in black and T183A in dotted gray lines (averaged over the two runs). (b) C_α-rms fluctuations (in Å) with respect to the average MD structure (wt in black, run 1 of T183A in gray, and run 2 in dotted gray).

TABLE 1: Properties of the Monomer of Wild-Type PrP and Its T183A Variant at 290 and 320 K[a]

		C_α-rmsd		native helices and β-strands				
T	PrP monomer	all	H2−H3	H1%	H2%	H3%	S1	S2
290 K	wild-type	4.3	0.8	99.9	99.9	95.4	+	+
	T183A run 1	5.5	5.2	99.9	92.7	99.0	+	−
	T183A run 2	4.9	2.0	99.9	99.8	68.3	+	+
320 K	wild-type	6.3	1.0	80.0	99.7	75.8	+	+
	T183A run 1	5.9	2.2	99.9	99.6	78.6	−	−
	T183A run 2	6.2	1.5	99.9	99.6	86.9	−	−

[a] The properties are calculated excluding the first 30 ns. The C_α-rmsd all is calculated using the amino acids 125−215, and C_α-rmsd H2−H3 using the amino acids 172−215. The time formation of helices H1 (spanning 144−153), H2 (spanning 172−192), and H3 (spanning 200−225) is calculated using STRIDE.[54] The last two columns indicate the presence (+) or absence (−) of the native strands S1 and S2.

native β-strands in T183A is consistent with their high dynamic character as observed by NMR relaxations measurements on wild-type PrP90-231,[56] although we cannot ignore that the absence of the region 90−124 in our simulations may impact the stability of the antiparallel β-sheet. Finally, the detection of a kink in helix H2 of T183A was also featured in the NMR structure of *Xenopus* leavis PrP at position 189.[6]

Similar time-averaged properties are found at 320 K in both species within 100 ns. As seen in Figure 3a, the rmsd plots superpose rather well on each other with deviations of 6−7 Å at 100 ns. The rmsd decomposition of the residues 125−215 in Table 1 reveals that the deviations result from the flexibility of the S1H1S2 subdomain and its reorientation with respect to the H2H3 subdomain, the rmsd for H2H3 and helix H1 is 2 and 1 Å, respectively, in both species. Despite these high rmsd values, the time formation of each native helix does not vary much between the simulations: helices H1 and H2 are both intact as seen in Table 1 and helix H3 is broken into two parts as shown by the secondary structure profiles in panels 3b and 3c. We see, however, local secondary structure variations. A non-native helix is formed 80% of the time in wild-type PrP at positions

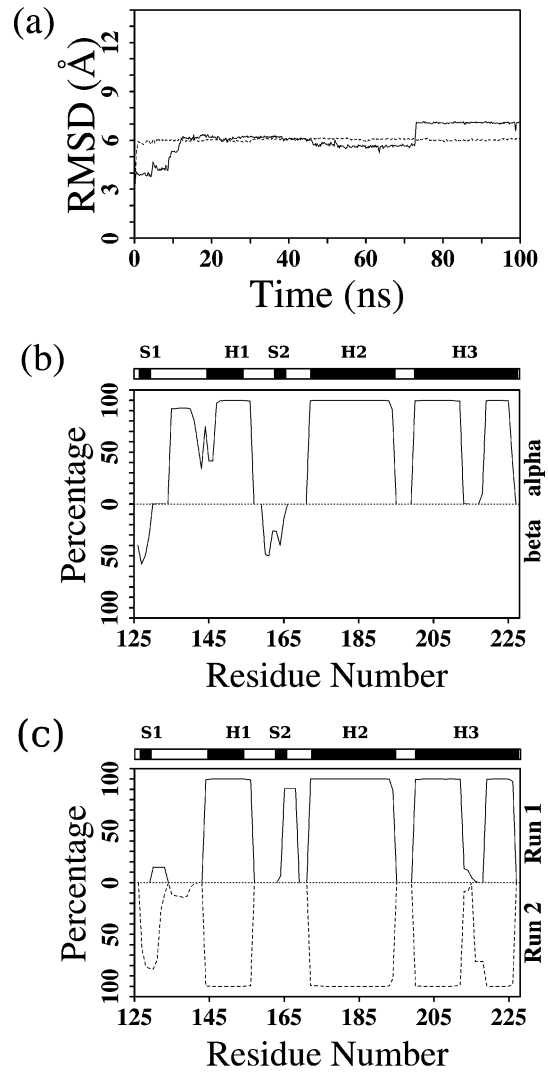

Figure 3. Properties at 320 K of the monomer of PrP wild-type and its T183A variant. (a) C_α-rmsd (in Å) from the minimized structure of the residues 129−215 for the wild-type in black and T183A in dotted gray lines (averaged over the two runs) (b,c) Secondary structure as a function of the amino acid index for wild-type (b) and T183A (c). While we show the β and α signal of wild-type in panel b, we only show the α signal in panel c (β-strand signal = 0%). The location of native S1, S2, H1, H2, and H3 are indicated by black boxes.

135−141 (S1−H1 loop) while non-native helices form 15% of the time at positions 130−133 (S1 location) in T183A run 1, and 80% of the time at positions 128−133 in T183 run 2. We also find a non-native α-helix in the S2−H2 loop (run 1, panel c). While the impact of force field parametrization cannot be neglected, the occurrence of non-native helix in the region 130−141 at 320 K (and 360 K, see below) does not run in contrast with the fact that the human PrP(128−145) peptide itself forms fibrils in vitro,[60] as non-native helices form prior to amyloid-β protein fibril assembly.[61] Looking at the β-strand signal, the native S1 and S2 are elongated in the wild-type run spanning residues 126−131 and 160−165 (vs 129−130 and 162−163 in native state) and formed 47% and 55% of the time. By contrast, the initial β-sheet is no longer conserved in the two runs of the variant, in agreement with metadynamics simulations of mouse PrP124-216 D178N.[28]

Overall, although our sampling cannot capture all fluctuations, we find that in both species helix H1 is very stable, helix H3 is very dynamic, and the S1H1S2 subdomain is mobile with respect to the H2H3 subdomain, and the α-helix signal does

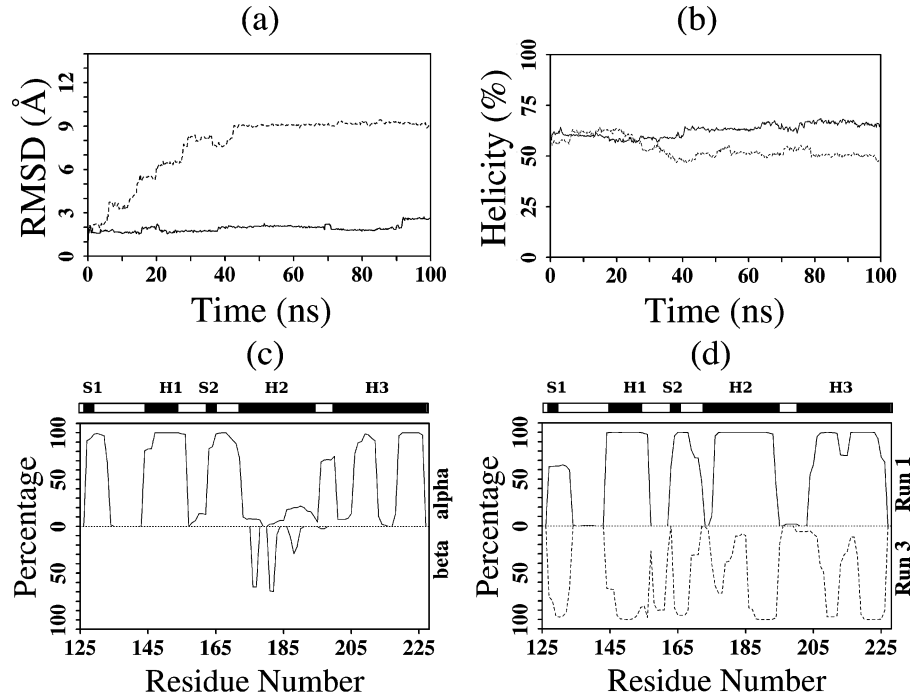

Figure 4. High-temperature (360 K) properties of the wild-type and T183A PrP monomers. Black lines correspond to wild-type and dotted gray lines to T183A in panels a and b. (a) C_α-rmsd (in Å) of the residues 172−215 from their starting positions, averaged over the three T183A runs and the two wild-type runs. (b) Percentage of α-helix as a function of time. (c,d) Secondary structure profiles as a function of the amino acid index in run 2 (c) and runs 1 and 3 (d) of T183A.

not vary much below T_m. This is consistent with REMD simulations of wild-type PrP,[53] and the similarity in the far-UV CD spectra of wild-type and T183A PrP at 298 K.[23]

3.2. H2H3 Subdomain in Wild-Type and T183A Monomer at 360 K. Here, we report the structural properties of wild-type PrP from two 100 ns runs and its T183A variant from three 100 runs at 360 K ($>T_m$). In Figure 4a we see that the H2H3 subdomain spanning residues 172−215 undergoes major structural changes in all runs of T183A, but not in wild-type PrP: the C_α-rmsd reaches 9 Å for T183A versus 2.6 Å for the wild-type at 100 ns. Calculated on the residues 125−215, the C_α-rmsd is 11 Å for the variant versus 7 Å for the wild-type. The mean percentage of α-helix content decreases by 10% in the variant (Figure 4b): 62.6% for the wild-type and 53.7% for T183A, as a result of the destabilization of the helices H2 and H3 in runs 2 and 3 (panels 4c and 4d). The helices H2 and H3 are, however, essentially formed in T183A run 1. Remarkably, helix H1 is found stable in the three T183A runs and is elongated by three residues (from Met154 to Arg156).

The propensity for disordered helices H2 and H3 in T183A is compensated by the formation of transient non-native helices at positions 127−133 in the S1H1S2 subdomain (runs 1, 2, and 3), at positions 163−172 in the S2−H2 loop (runs 1, 2, and 3) and at positions 196−200 in the loop between H2 and H3 (run 2). These new helices are formed, however, in the regions that are experimentally known to be flexible: the strands S1 and S2 and the loop H2−H3,[56] and the S2−H2 loop.[11] The initial β-sheet is no longer conserved in the three runs of the variant.

In Figure 5, we superpose the most populated conformations, excluding the first 30 ns of all simulations, on the wild-type experimental structure. The centers of the two clusters for wild-type PrP in Figure 5a−5b, with a population of 33% and 42%, display molten globule-like properties: the subdomain covering the full-length H2 and N-terminal H3 helices is stable (C_α-rmsd of 2.3 Å in runs 1 and 2) and helix H1 is reorientated with respect to the H2H3 subdomain. Figure 5b also shows the formation of non-native helices spanning S1 and the S2−H2 loop. In contrast to wild-type PrP, the most populated clusters of T183A are predominantly disordered (panels 5d, 5e, and 5f with populations of 22%, 7%, and 19%, respectively), although the molten globule state is still populated (22%, panel 5c). Notably, in run 2 of T183A, the unwinding of helix H2 and of the N-terminal H3 helix allows for the formation of a two- or three-stranded β-sheet, at positions 176−177 and 181−182 (Figure 5d) and at positions 176−177, 181−182, and 187−188 (Figure 5e), respectively.

Overall, the higher thermal vibrations from the experimental MD average structure and the higher ratio of disordered than molten globule states at 360 K in T183A PrP with respect to wild-type PrP indicate that the melting temperature of T183A PrP is lower than that of wild-type PrP. This is in agreement with urea-induced equilibrium transition experiments.[23]

It has been hypothesized that the loss of the two hydrogen bonds upon T183A mutation between Tyr162-H(N) and Thr183-OH, and Thr183-H(N) and Cys179-O(C) destabilizes the C-terminal core of the protein.[22] We find that replacement of Thr by Ala at $T > T_m$ destabilizes local side-chain−side-chain interactions with Val180, Gln186, and His187, but also long-range sequence interactions with Val161, Tyr162, and Val210. While H2 and H3 helices are likely to be more disordered in T183A PrP than in wild-type PrP and form transient non-native β-sheet in the H2 region at $T > T_m$, helix H1 is remarkably stable and is detached from the H2H3 core in all simulations.

3.3. Effects of T183A on PrP Dimers above T_m. Excluding the first 10 ns, all MD-generated conformations of the dimer T183 runs at 360 K ($>T_m$) can be clustered into three equally populated conformations of 25% (Figure 5g−i). All of them display stable H1 and N-terminal H3 helices and a fully destabilized native β-sheet. They differ, however, in two respects. First, helix H2 can be either fully formed in one chain and destabilized in the other (Figure 5g and 5h) or fully formed in both chains (Figure 5i). Second, intermolecular β-sheets

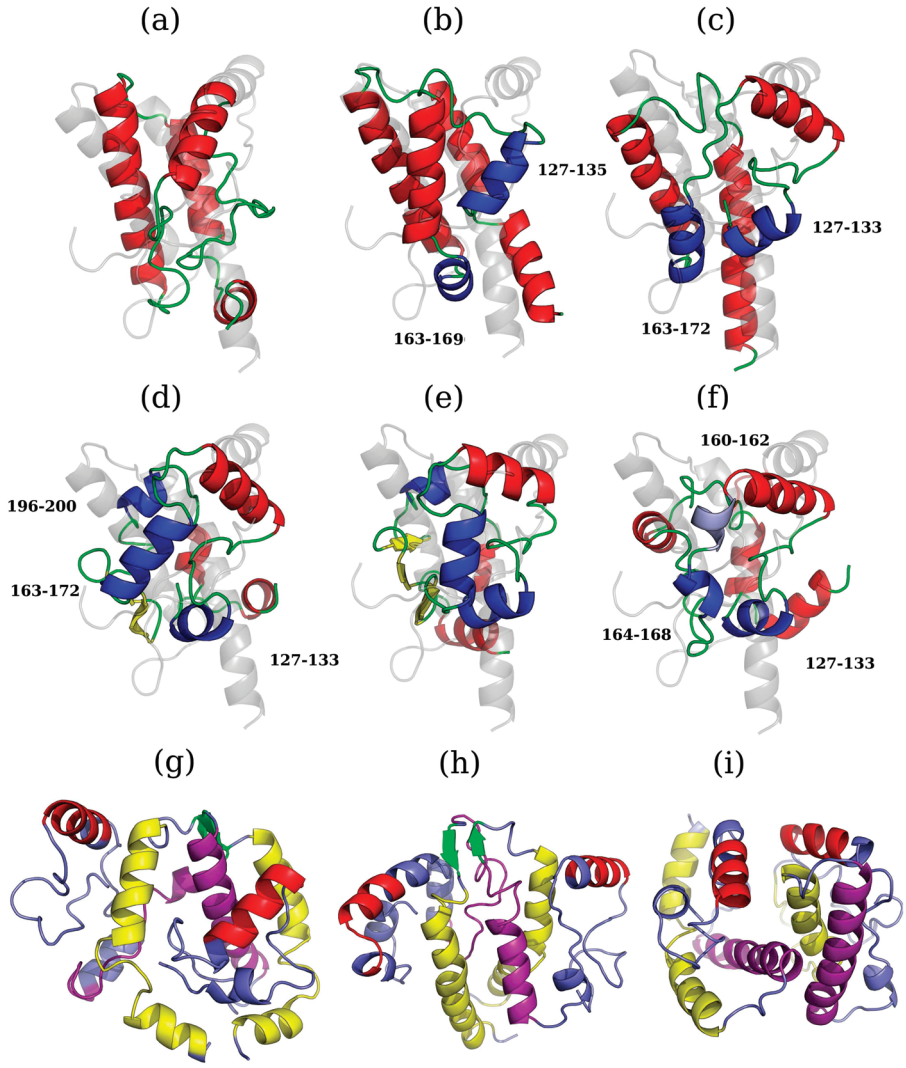

Figure 5. Dominant clusters of wild-type and T183A PrP monomer and T183A PrP dimer at 360 K superposed on the native wild-type recPrP structure. In panels a−f, the native wild-type structure is in shaded gray: (a,b) runs 1 and 2 of wild-type monomer; (c) run 1 of T183A monomer; (d,e) run 2 of T183A monomer; (f) run 3 of T183A monomer; (g−i) runs 1, 2, and 3 of T183A dimer. In all panels, Helix 1 is in red, H2 in purple, and H3 in yellow, non-native helices are in blue, and non-native β-sheets are in green. In panels b,c, the positions of non-native helices are also indicated.

between H2 and H3 form in two runs among three, spanning amino acids 193−194 and 197−198 (run 1, panel 5g) and 191−193 and 197−198 (run 2, panel 5h).

Although an intermolecular two-stranded β-sheet spanning residues 191−193 is displayed in the helix-swapped human crystal structure with an intermolecular disulfide bridge,[62] and discussed in all-atom MD simulations of PrP119−226 dimer at 500 K starting from the same state with the swapping of helix H3,[34] here we use the structure free of any domain swapping.

To study the impact of temperature and mutation T183A on the formation of intermolecular β-sheets, we conducted three 60 ns runs on wild-type dimer at 360 K and three 60 ns runs on T183A dimer at 320 K. Interestingly, all the simulations do not display any intermolecular β-sheet in the H2−H3 loop. Supporting Information Figure S1 shows the four dominant cluster centers of the wild-type dimer at 360 K with populations of 16% (panel a), 19% (panel b), and 11% each (panels c and d). Comparison of these centers with those of the wild-type monomer at the same temperature reveals that H1 is stable and intermolecular β-sheets form in two runs among three at positions 142−143 and 226−227 (panels b−d). These results suggest that the rate-limiting factor for the formation of intermolecular β-sheet in the H2−H3 loop of wild-type PrP is thermodynamics rather than kinetics. More importantly, all the simulations indicate that the populations of intermolecular sheets are likely to be negligible at low temperatures and neutral pH.

It is also important to determine whether common intramolecular properties are shared by the T183A monomer and dimer simulations above T_m. We find that both instances features a negligible population of native strands S1 and S2, an extension of helix H1 (until residue 155, 156, or 160 in the dimer vs residue 156 in the monomer), a partial or total destabilization of helix H2, and a kinked helix H3 at position 215.

4. Discussion and Conclusions

Characterization of the aggregation-prone intermediate monomeric and dimeric states is an essential aspect in understanding the transconformation of PrP from PrP^C or recPrP to PrP^{Sc}. In this study, using coarse-grained protein molecular dynamics, we have investigated the structural and dynamic properties of the recombinant sheep prion protein PrP125−228 and its CJD-causing T183A variant. There is experimental evidence that the point mutation T183A reduces recPrP121-231 stability without any changes in α-helix contents at 290 K.[23]

Although coarse-graining of the side-chains and the implicit solvent model simplify the energy landscape and cannot reproduce exactly the structural and dynamics properties of all-atom simulations in explicit solvent, they allow the exploration of much longer time scales, thereby providing insights into generic properties of oligomeric intermediates.

Overall, our simulations at 290 K show that the monomers of wild-type and T183A PrP display similar α-helix signals, consistent with far-UV CD spectra.[23] Although the C-terminal helix H3 and the strands S1 and S2 are much more mobile in T183A than in wild-type, the PrP tertiary structure does not change much upon T183A mutation, in agreement with near-UV CD spectra of murine PrP121-231 and its T183A variant at 298 K.[23] This difference on dynamics but not on mean structure has been noted on oxidation mutants of PrP at room temperature.[63]

PrP^{Sc} formation involves a substantial increase in β-strand content. From the monomer simulations at 320 K ($<T_m$), accelerating conformational sampling, but favoring the native state, we do not find any β-rich structures. Instead, the wild-type PrP monomer displays structural characteristics of molten globules, while the monomer of T183A has a higher ratio of disordered than molten globule states. This result for wild-type PrP is consistent with NMR experiments, assessed through low pH[64] or high pressure[65] conditions, and all-atom MD simulations of Syrian hamster PrP90-231.[24]

Increasing the temperature above T_m, we find that the subdomain H2H3 is disordered in the T183A monomer, but not in the wild-type monomer. This agrees with the experimental decrease in PrP thermodynamic stability upon T183A mutation.[23] The destabilization results from a high conformational flexibility of either the full helix H2, the N-terminal end of helix H2, or the N-terminal end of H3. The high unfolding propensity of helices H2 and H3 is also observed in the dimer of T183A at 360 K, albeit their destabilization is not systematic (H2 remains formed in run 2). This instability of helix H2 is in line with previous simulations[24,26,66] and its unusual amyloidogenic property.[67,68]

Remarkably, we find that helix H1 remains stable and even elongates at its C-terminal end in the monomer and dimer of both sequences, independently of T. The strong preference of the amino acids 143−156 for α-helix has been demonstrated by NMR on several peptides encompassing H1 under different pH and solvent conditions[69] and all-atom simulations of helix H1[15,26] using distinct molecular force fields. The high stability of helix H1 and its elongation have also been recently discussed by all-atom REMD simulations of sheep PrP125-230 monomer in explicit solvent.[53] Nevertheless, there is compelling numerical evidence that H1 may not retain its full length under all pathogenic conditions, helix H1 spanning only amino acids 145−149 in simulations of Syrian hamster PrP90-231 with deletion of strand S1.[24] This possibility of shorter H1 helix was also proposed by comparing the CD signals of human PrP23-159 and PrP23-144 fibrils.[70]

To summarize, our work in conjunction with recent experimental and theoretical results have three implications on our knowledge of both monomeric and dimeric intermediates: (i) the native β-sheet is either weakened or elongated by pathogenic mutations,[28,29] (ii) the detachment of the S1H1S2 domain from the H2H3 subdomain is a generic property of wild-type PrP[53,71,72] and most variants. (iii) the H2H3 subdomain is in equilibrium between a fully formed α-helical hairpin and many states of reduced helical contents and specifically of low helicity in the C-terminal region of H2 under denaturing conditions, and displays a marginally populated β-sheet content.

Our simulations go one step ahead of all previous PrP simulations and the available experimental data, by providing strong evidence that helix H1 is retained and the H2H3 subdomain has very little intermolecular β-sheet structure in the dimer intermediates. Whether, in the late steps of aggregation, H1 converts into a β-helix and H2H3 remains helical, as suggested by the PrP^{Sc} model of Wille et al.,[73] or H1 remains formed and the H2H3 subdomain is part of the cross-β core, as suggested by the PrP^{Sc} model of Surewicz et al.,[74,75] cannot be established here. According to these PrP^{Sc} models, either H1 or H2H3 has, however, to convert to β-sheet in the higher order oligomers en route to amyloid fibril formation. In this context, determination of the free energy barriers separating α-helices to β-sheets for trimers and higher oligomers of the peptides encompassing H1 and H2H3 would be of great help. We are currently calculating these free energy maps with OPEP REMD simulations.

Acknowledgment. P.D. is supported by the Centre National de la Recherche Scientifique, the Université Paris Diderot-Paris 7 and the European Grant "ImmunoPrion, FP6-Food-023144, 2006−2009".

Supporting Information Available: Figure S1: Dominant clusters of wild-type PrP dimer at 360 K (a) run 1, (b) run 2, (c,d) run 3. In all panels, helix 1 is in red, H2 in purple, and H3 in yellow, non-native helices are in blue, and non-native β-sheets in green. In panels b-d, the positions of intermolecular β-sheets are indicated. This material is available free of charge via the Internet at http://pubs.acs.org.

References and Notes

(1) Prusiner, S. B.; McKinley, M. P.; Bowman, K. A.; Bolton, D. C.; Bendheim, P. E.; Groth, D. F.; Glenner, G. G. *Cell* **1983**, *35*, 349–358.
(2) Jackson, G. S.; Murray, I.; Hosszu, L. L.; Gibbs, N.; Waltho, J. P.; Clarke, A. R.; Collinge, J. *Proc. Natl. Acad. Sci. U.S.A.* **2001**, *98*, 8531–8535.
(3) Isaacs, J. D.; Jackson, G. S.; Altmann, D. M. *Clin. Exp. Immunol.* **2006**, *146*, 1–8.
(4) Pan, K. M.; Baldwin, M.; Nguyen, J.; Gasset, M.; Serban, A.; Groth, D.; Mehlhorn, I.; Huang, Z.; Fletterick, R. J.; Cohen, F. E. *Proc. Natl. Acad. Sci. U.S.A.* **1993**, *90*, 10962–10966.
(5) James, T. L.; Liu, H.; Ulyanov, N. B.; Farr-Jones, S.; Zhang, H.; Donne, D. G.; Kaneko, K.; Groth, D.; Mehlhorn, I.; Prusiner, S. B.; Cohen, F. E. *Proc. Natl. Acad. Sci. U.S.A.* **1997**, *94*, 10086–10091.
(6) Calzolai, L.; Lysek, D. A.; Perez, D. R.; Guntert, P.; Wuthrich, K. *Proc. Natl. Acad. Sci. U.S.A.* **2005**, *102*, 651–655.
(7) Eberl, H.; Tittmann, P.; Glockshuber, R. *J. Biol. Chem.* **2004**, *279*, 25058–25065.
(8) Elfrink, K.; Ollesch, J.; Stohr, J.; Willbold, D.; Riesner, D.; Gerwert, K. *Proc. Natl. Acad. Sci. U.S.A.* **2008**, *105*, 10815–10819.
(9) Baskakov, I. V.; Legname, G.; Prusiner, S. B.; Cohen, F. E. *J. Biol. Chem.* **2001**, *276*, 19687–19690.
(10) Soto, C. *Proc. Natl. Acad. Sci. U.S.A.* **2009**, *106*, 10–11.
(11) Sigurdson, C. J.; Nilsson, K. P. R.; Hornemann, S.; Heikenwalder, M.; Manco, G.; Schwarz, P.; Ott, D.; Rolicke, T.; Liberski, P. P.; Julius, C.; Falsig, J.; Stitz, L.; Wuthrich, K.; Aguzzi, A. *Proc. Natl. Acad. Sci. U.S.A.* **2009**, *106*, 304–309.
(12) Apetri, A. C.; Maki, K.; Roder, H.; Surewicz, W. K. *J. Am. Chem. Soc.* **2006**, *128*, 11673–11678.
(13) Bellinger-Kawahara, C. G.; Kempner, E.; Groth, D.; Gabizon, R.; Prusiner, S. B. *Virology* **1988**, *164*, 537–541.
(14) Kelly, J. W. *Curr. Opin. Struct. Biol.* **1998**, *8*, 101–106.
(15) Morrissey, M. P.; Shakhnovich, E. I. *Proc. Natl. Acad. Sci. U.S.A.* **1999**, *96*, 11293–11298.
(16) Kaimann, T.; Metzger, S.; Kuhlmann, K.; Brandt, B.; Birkmann, E.; Holtje, H.-D.; Riesner, D. *J. Mol. Biol.* **2008**, *376*, 582–596.
(17) Stohr, J.; Weinmann, N.; Wille, H.; Kaimann, T.; Nagel-Steger, L.; Birkmann, E.; Panza, G.; Prusiner, S. B.; Eigen, M.; Riesner, D. *Proc. Natl. Acad. Sci. U.S.A.* **2008**, *105*, 2409–2414.

(18) Dourmashkin, R. R.; Oxford, J. S.; Bountiff, L. *J. Neuropathol. Exp. Neurol.* **2004**, *63*, 32–42.
(19) Collinge, J. *Annu. Rev. Neurosci.* **2001**, *24*, 519–550.
(20) Nitrini, R.; Rosemberg, S.; Passos-Bueno, M. R.; da Silva, L. S.; Iughetti, P.; Papadopoulos, M.; Carrilho, P. M.; Caramelli, P.; Albrecht, S.; Zatz, M.; LeBlanc, A. *Ann. Neurol.* **1997**, *42*, 138–146.
(21) Grasbon-Frodl, E.; Lorenz, H.; Mann, U.; Nitsch, R. M.; Windl, O.; Kretzschmar, H. A. *Acta Neuropathol.* **2004**, *108*, 476–484.
(22) Kiachopoulos, S.; Bracher, A.; Winklhofer, K. F.; Tatzelt, J. *J. Biol. Chem.* **2005**, *280*, 9320–9329.
(23) Liemann, S.; Glockshuber, R. *Biochemistry* **1999**, *38*, 3258–3267.
(24) Santini, S.; Derreumaux, P. *Cell. Mol. Life Sci.* **2004**, *61*, 951–960.
(25) DeMarco, M. L.; Daggett, V. *Proc. Natl. Acad. Sci. U.S.A.* **2004**, *101*, 2293–2298.
(26) Dima, R. I.; Thirumalai, D. *Proc. Natl. Acad. Sci. U.S.A.* **2004**, *101*, 15335–15340.
(27) Shamsir, M. S.; Dalby, A. R. *Proteins* **2005**, *59*, 275–290.
(28) Barducci, A.; Chelli, R.; Procacci, P.; Schettino, V.; Gervasio, F. L.; Parrinello, M. *J. Am. Chem. Soc.* **2006**, *128*, 2705–2710.
(29) Santini, S.; Claude, J.-B.; Audic, S.; Derreumaux, P. *Proteins* **2003**, *51*, 258–265.
(30) Gorfe, A. A.; Caflisch, A. *FASEB J.* **2007**, *21*, 3279–3287.
(31) Langella, E.; Improta, R.; Crescenzi, O.; Barone, V. *Proteins* **2006**, *64*, 167–177.
(32) Colacino, S.; Tiana, G.; Colombo, G. *BMC Struct. Biol.* **2006**, *6*, 17.
(33) Settanni, G.; Hoang, T. X.; Micheletti, C.; Maritan, A. *Biophys. J.* **2002**, *83*, 3533–3541.
(34) Sekijima, M.; Motono, C.; Yamasaki, S.; Kaneko, K.; Akiyama, Y. *Biophys. J.* **2003**, *85*, 1176–1185.
(35) Derreumaux, P. *Biophys. J.* **2001**, *81*, 1657–1665.
(36) Langedijk, J. P. M.; Fuentes, G.; Boshuizen, R.; Bonvin, A. M. J. J. *J. Mol. Biol.* **2006**, *360*, 907–920.
(37) Pushie, M. J.; Vogel, H. J. *Biophys. J.* **2007**, *93*, 3762–3774.
(38) Pearlman, D.; Case, D.; Caldwell, J.; Ross, W.; Cheatham, I.; DeBolt, S.; Ferguson, D.; Seibel, G.; Kollman, P. *Comput. Phys. Commun.* **1995**, *91*, 1–41.
(39) Derreumaux, P. *J. Chem. Phys.* **1999**, *111*, 2301–2310.
(40) Forcellino, F.; Derreumaux, P. *Proteins* **2001**, *45*, 159–166.
(41) Derreumaux, P.; Mousseau, N. *J. Chem. Phys.* **2007**, *126*, 025101.
(42) Maupetit, J.; Tuffery, P.; Derreumaux, P. *Proteins* **2007**, *69*, 394–408.
(43) Chen, W.; Mousseau, N.; Derreumaux, P. *J. Chem. Phys.* **2006**, *125*, 084911.
(44) Chebaro, Y.; Dong, X.; Laghaei, R.; Derreumaux, P.; Mousseau, N. *J. Phys. Chem. B* **2009**, *113*, 267–274.
(45) Santini, S.; Wei, G.; Mousseau, N.; Derreumaux, P. *Structure* **2004**, *12*, 1245–1255.
(46) Melquiond, A.; Boucher, G.; Mousseau, N.; Derreumaux, P. *J. Chem. Phys.* **2005**, *122*, 174904.
(47) Haire, L. F.; Whyte, S. M.; Vasisht, N.; Gill, A. C.; Verma, C.; Dodson, E. J.; Dodson, G. G.; Bayley, P. M. *J. Mol. Biol.* **2004**, *336*, 1175–1183.
(48) Arnold, K.; Bordoli, L.; Kopp, J.; Schwede, T. *Bioinformatics* **2006**, *22*, 195–201.
(49) Forloni, G.; Angeretti, N.; Chiesa, R.; Monzani, E.; Salmona, M.; Bugiani, O.; Tagliavini, F. *Nature (London)* **1993**, *362*, 543–546.
(50) Tagliavini, F.; Prelli, F.; Verga, L.; Giaccone, G.; Sarma, R.; Gorevic, P.; Ghetti, B.; Passerini, F.; Ghibaudi, E.; Forloni, G. *Proc. Natl. Acad. Sci. U.S.A.* **1993**, *90*, 9678–9682.
(51) Rezaei, H.; Marc, D.; Choiset, Y.; Takahashi, M.; Hoa, G. H. B.; Haertl, T.; Grosclaude, J.; Debey, P. *Eur. J. Biochem.* **2000**, *267*, 2833–2839.
(52) DeMarco, M. L.; Daggett, V. *Biochemistry* **2007**, *46*, 3045–3054.
(53) Simone, A. D.; Zagari, A.; Derreumaux, P. *Biophys. J.* **2007**, *93*, 1284–1292.
(54) Frishman, D.; Argos, P. *Proteins* **1995**, *23*, 566–579.
(55) Spoel, D. V. D.; Lindahl, E.; Hess, B.; Groenhof, G.; Mark, A. E.; Berendsen, H. J. C. *J. Comput. Chem.* **2005**, *26*, 1701–1718.
(56) Viles, J. H.; Donne, D.; Kroon, G.; Prusiner, S. B.; Cohen, F. E.; Dyson, H. J.; Wright, P. E. *Biochemistry* **2001**, *40*, 2743–2753.
(57) Huet, A.; Derreumaux, P. *Biophys. J.* **2006**, *91*, 3829–40.
(58) Hosszu, L. L.; Baxter, N. J.; Jackson, G. S.; Power, A.; Clarke, A. R.; Waltho, J. P.; Craven, C. J.; Collinge, J. *Nat. Struct. Biol.* **1999**, *6*, 740–743.
(59) Calzolai, L.; Lysek, D. A.; Guntert, P.; von Schroetter, C.; Riek, R.; Zahn, R.; Wuthrich, K. *Proc. Natl. Acad. Sci. U.S.A.* **2000**, *97*, 8340–8345.
(60) Ziegler, J.; Viehrig, C.; Geimer, S.; Rosch, P.; Schwarzinger, S. *FEBS Lett.* **2006**, *580*, 2033–2040.
(61) Kirkitadze, M.; Condron, M.; Teplow, D. *J. Mol. Biol.* **2001**, *312*, 1103–19.
(62) Knaus, K. J.; Morillas, M.; Swietnicki, W.; Malone, M.; Surewicz, W. K.; Yee, V. C. *Nat. Struct. Biol.* **2001**, *8*, 770–774.
(63) Colombo, G.; Meli, M.; Morra, G.; Gabizon, R.; Gasset, M. *PloS ONE* **2009**, *4*, e4296.
(64) Gerber, R.; Tahiri-Alaoui, A.; Hore, P. J.; James, W. *J. Biol. Chem.* **2007**, *282*, 6300–6307.
(65) Kuwata, K.; Li, H.; Yamada, H.; Legname, G.; Prusiner, S. B.; Akasaka, K.; James, T. L. *Biochemistry* **2002**, *41*, 12277–12283.
(66) Fitzmaurice, T. J.; Burke, D. F.; Hopkins, L.; Yang, S.; Yu, S.; Sy, M.-S.; Thackray, A. M.; Bujdoso, R. *Biochem. J.* **2008**, *409*, 367–375.
(67) Yamaguchi, K.-I.; Matsumoto, T.; Kuwata, K. *Biochemistry* **2008**, *47*, 13242–13251.
(68) Ronga, L.; Palladino, P.; Ragone, R.; Benedetti, E.; Rossi, F. *J. Pept. Sci.* **2009**, *15*, 30–35.
(69) Ziegler, J.; Sticht, H.; Marx, U. C.; Muller, W.; Rosch, P.; Schwarzinger, S. *J. Biol. Chem.* **2003**, *278*, 50175–50181.
(70) Watzlawik, J.; Skora, L.; Frense, D.; Griesinger, C.; Zweckstetter, M.; Schulz-Schaeffer, W. J.; Kramer, M. L. *J. Biol. Chem.* **2006**, *281*, 30242–30250.
(71) Eghiaian, F.; Daubenfeld, T.; Quenet, Y.; van Audenhaege, M.; Bouin, A.-P.; van der Rest, G.; Grosclaude, J.; Rezaei, H. *Proc. Natl. Acad. Sci. U.S.A.* **2007**, *104*, 7414–7419.
(72) Schwarzinger, S.; Horn, A. H.; Ziegler, J.; Sticht, H. *J. Biomol. Struct. Dyn.* **2006**, *23*, 1–10.
(73) Govaerts, C.; Wille, H.; Prusiner, S. B.; Cohen, F. E. *Proc. Natl. Acad. Sci. U.S.A.* **2004**, *101*, 8342–8347.
(74) Lu, X.; Wintrode, P. L.; Surewicz, W. K. *Proc. Natl. Acad. Sci. U.S.A.* **2007**, *104*, 1510–1515.
(75) Cobb, N. J.; Sonnichsen, F. D.; McHaourab, H.; Surewicz, W. K. *Proc. Natl. Acad. Sci. U.S.A.* **2007**, *104*, 18946–18951.

JP900334S